metals

MDPI

Article

On Glass Forming Ability of Bulk Metallic Glasses by Relating the Internal Friction Peak Value

Xianfeng Zhang [1], Xiao Cui [1,2,*], Zhuotong Du [1], Fangqiu Zu [3,*], Jinjing Li [2], Bingchuan Bian [2], Kuilong Xu [1] and Xinyao Zhang [1,4]

1 Luoyang Ship Material Research Institute, Luoyang 471023, China; zhangxianfeng0811@163.com (X.Z.); duzhuotong123@163.com (Z.D.); xukuilong@sina.com (K.X.); 13525971194@163.com (X.Z.)
2 College of Mechanical and Architectural Engineering, Taishan University, Taian 271000, China; lijinjing@tsu.edu.cn (J.L.); bianbingchuan@163.com (B.B.)
3 Institute of Liquid/Solid Metal Processing, School of Materials Science & Engineering, Hefei University of Technology, Hefei 230009, China
4 Henan Key Laboratory of Technology and Application of Structural Materials for Ships and Marine Equipments, Luoyang 471023, China
* Correspondence: xcui@live.com (X.C.); fangqiuzu@hotmail.com (F.Z.); Tel.: +86-053-867-155-53 (X.C); +86-055-162-905-057 (F.Z.)

Received: 7 May 2020; Accepted: 6 June 2020; Published: 9 June 2020

Abstract: The internal friction (IF) behaviors of a series of LaCe-, Zr-, and La-based bulk metallic glasses (BMGs) were studied by a computer-controlled, conventional inverted torsion pendulum. The results indicate that with an increasing temperature, the IF also increases gradually in the supercooled liquid region, followed by a decrease caused by crystallization. BMGs with a good glass forming ability (GFA) usually possess a high IF peak value for an alloy system with the same constituent elements. Furthermore, the magnitude of the IF value (Q_i^{-1}) of the inflection point is an efficient criterion of GFA. The Q_i^{-1} value is a valid criterion under the conditions of identical constituent elements and different element contents. However, Q_i^{-1} and GFA have no relationship among different alloy systems.

Keywords: bulk metallic glasses; glass forming ability; internal friction; inflection point; supercooled liquid region

1. Introduction

Internal friction (IF) is a structure-sensitive physical quantity of materials and can be described as a vibrating solid in which its mechanical vibration gradually decays even when completely isolated from the outside space [1–6]. Mechanical energy dissipating into thermal energy is called IF. In an IF measurement, most glassy materials are viscoelastic and exhibit an angle δ by which the strain lags behind the stress [7]. On the basis of the relationship of the lag angle δ and the amplitudes of the stress and strain waves, a series of fundamental parameters of glassy materials can be determined; such parameters include the storage modulus E', loss modulus E'', and loss tangent $tan\delta$ (also called the IF of the materials, which is defined as Q^{-1} and expressed as $Q^{-1} = tan\delta$ [7]). IF technology is sensitive to point defects and phase transformations in solid materials [8–11]. However, bulk metallic glass (BMG) constitutes a man-made non-crystalline state [12]. IF technology can also be used to study the structural relaxation, glass transition, and crystallization behaviors of amorphous alloys [13–23].

An IF peak usually appears within the temperature range of crystallization during BMG heating. However, many controversies have arisen about the origin of IF peaks. A cluster model has been proposed to explain the formation of IF peaks for amorphous alloys; IF is related to the shear motion of clusters in the amorphous alloys and the number and size of the clusters [4]. At an appropriate

temperature near T_g, the maximum IF value is attained when the atoms reach their critical size and number. IF continues to increase in a supercooled liquid region above T_g [3,22], and IF peaks originate from the beginning of crystallization. Zhang et al. [23] considered that IF peak formation during heating is the result of a combined action of glass transition and crystallization.

A preliminary exploration was conducted on the relationship between the IF peak and glass forming ability (GFA). Zhang et al. [23] found that the IF peak of $Zr_{57}Al_{10}Ni_{12.4}Cu_{15.6}Nb_5$ BMG is higher than that of $Pd_{80}Si_{20}$ and $Ni_{74}P_{16}B_6Al_4$ MGs. This result implies that the IF peak of BMGs is related to their GFA. However, this conclusion lacks a systematic summary of the relationship between same alloy systems and different alloy systems. Different groups have proposed various GFA criteria, such as a supercooled liquid region (ΔT_x) [24], reduced glass transition temperature (T_{rg}) [25], parameter γ [26], and electrical resistivity [27]. Under different research conditions, an expanding novel GFA criterion will be helpful for exploring new alloy compositions with excellent GFA. As an efficient parameter that is sensitive to the structure of BMGs, exploring the relationship between the IF value and GFA will be useful for realizing the essence of GFA.

In this study, a series of BMGs with different GFA, including Zr-, La-, and LaCe-based BMGs, was manufactured. IF was measured to investigate their variation trend from a glass state to a supercooled liquid and a crystallized form. The mechanism of IF peak formation and the inherent relationship between IF and GFA were also discussed.

2. Experimental Procedure

Master ingots with a nominal composition of $Zr_{44}Cu_{40}Al_8Ag_8$ [28], $Zr_{46}Cu_{38}Al_8Ag_8$ [28], $Zr_{48}Cu_{36}Al_8Ag_8$ [28], $Zr_{48}Cu_{34}Pd_2Al_8Ag_8$ [28], $Zr_{46}Cu_{30.14}Ag_{8.36}Al_8Be_{7.5}$ [29], $La_{66}Al_{14}Cu_{10}Ni_{10}$ [30], $La_{62}Al_{14}Cu_{12}Ni_{12}$ [30], $La_{65}Al_{14}Cu_{9.167}Ag_{1.833}Ni_5Co_5$ [31], $(La_{0.3}Ce_{0.7})_{65}Al_{10}Co_{25}$ [32], $(La_{0.5}Ce_{0.5})_{65}Al_{10}Co_{25}$ [32], $(La_{0.4}Ce_{0.6})_{65}Al_{10}Co_{25}$ [32], $(La_{0.7}Ce_{0.3})_{65}Al_{10}Co_{25}$ [32], and $(La_{0.8}Ce_{0.2})_{65}Al_{10}Co_{25}$ [32] were prepared by arc melting in high purity argon atmosphere; during the melting, elements of high purity were used (99.5% for La and Ce, at least 99.9% for other elements). The arc melting was performed in high purity Argon atmosphere. The ingot was re-melted five times in the arc melter, accompanied with electromagnetic stirring in order to ensure chemical homogeneity.

Plane samples with a dimension of $1.2 \times 5 \times 100$ mm^3 were manufactured using the copper mold suction casting method. The structures of the samples were characterized by X-ray diffraction (XRD) with the Cu-Kα radiation. The samples used for the IF measurement were cut into thin strips with a dimension of $1.2 \times 2 \times 55$ mm^3. The IF measurement was performed using a conventional inverted torsion pendulum controlled by a computer with an error of about 10^{-3}, and the driving frequencies used in the IF measurement were 0.5 Hz, 1 Hz, 3 Hz, and 10 Hz, respectively. The temperature ranges for the IF measurement were determined by the crystallization temperature (T_x) and melt temperature (T_m), and each specimen was heated from room temperature to 550 K. In this work, the heating rate for the IF measurement was 1 K/min.

3. Results

Figure 1 shows the X-ray diffraction patterns of plane shape BMG samples prepared via copper mold suction casting. All samples show a large broad peak on the diffraction curve, and for all samples no diffraction peaks corresponding to crystalline phases can be observed, which indicates that all the prepared samples are in the amorphous state.

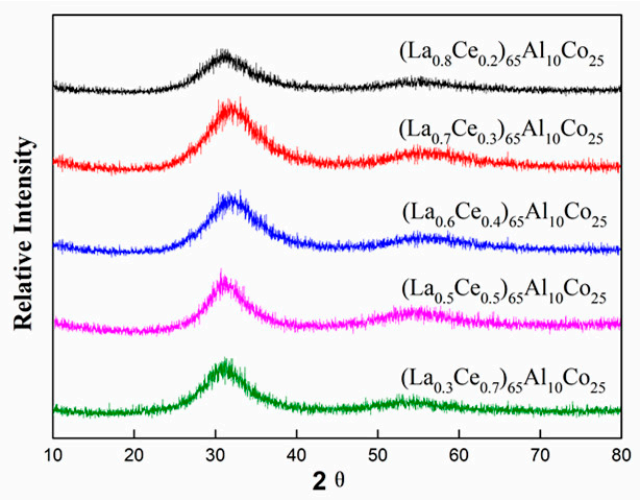

Figure 1. XRD (*X*-ray diffraction) patterns of the as-cast LaCe-based BMGs (bulk metallic glasses).

Figure 2a–e presents the Q^{-1}–T curves of LaCe-based BMGs with driving frequencies of 0.5 Hz, 1 Hz, 3 Hz, and 10 Hz. The Q^{-1}–T curves of LaCe-based BMGs with respect to the temperature have three characteristic regions. In region I, BMGs are in a complete glassy state from room temperature to approximately 400 K, and Q^{-1} is almost independent of the increasing temperature; however, remarkable humps called slow β relaxation [33] can be observed in this region. In region II, Q^{-1} initially increases slightly and then increases rapidly until the maximum value is reached from 400 K to approximately 450 K; the corresponding temperature of the maximum value appearing in the Q^{-1}–T curves usually corresponds to the beginning of crystallization [34]. In region III, Q^{-1} begins to decrease from approximately 450 K to 500 K, indicating the crystallization of BMGs.

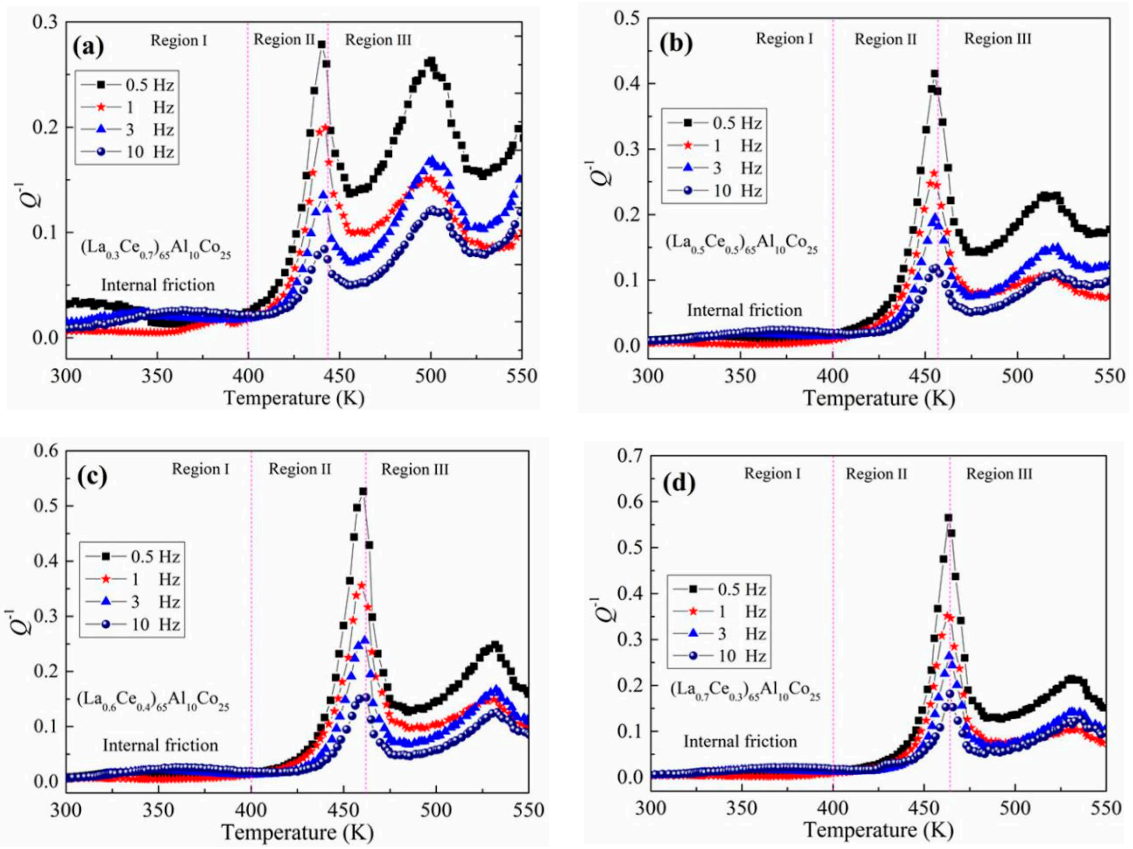

Figure 2. *Cont.*

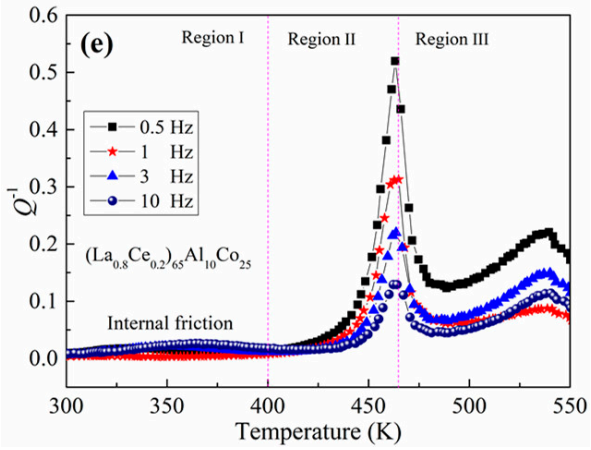

Figure 2. (**a–e**) Q^{-1}–T curves of the as-cast LaCe-based BMGs with driving frequencies of 0.5 Hz, 1 Hz, 3 Hz, and 10 Hz, respectively.

Figure 2a–e also illustrates that the IF at a given temperature is dependent on the driving frequency; that is, the lower the driving frequency, the higher the IF. Additionally, the IF peak temperature is nearly independent of the driving frequency. Q^{-1}–T curves with driving frequencies of 0.5 Hz and 1 Hz are merged into one diagram to compare IF with respect to the GFA of LaCe-based BMGs, as shown in Figure 3a,b. Figure 3a,b further reveals that the extent of the quantitative value increases as the driving frequency decreases. As a result, a low error is obtained when the relationship between IF and GFA is compared. For the LaCe-based BMGs in this work, the components are identical, but their La/Ce ratio is different. As shown in Table 1, the GFA of the LaCe-based BMGs increases gradually with the La content; a maximum value of 25 mm can be obtained when the La/Ce ratio is 7/3. The GFA decreases when the La/Ce ratio is greater than 7/3 [31].

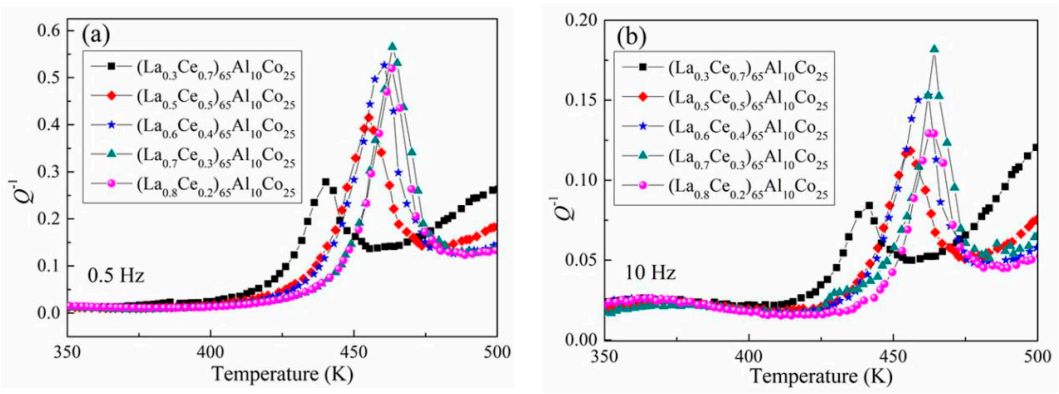

Figure 3. Comparison of the Q^{-1}–T curves of the LaCe-based BMGs with the driving frequencies of (**a**) 0.5 Hz and (**b**) 10 Hz, respectively.

Table 1. The GFA parameters (Dc [32], T_g [32], T_x [32], ΔT_x [32], T_{rg} [32], and γ [32]), IF peak values ($Q_p{}^{-1}$) with a driving frequency of 0.5 Hz, and inflection point IF values ($Q_i{}^{-1}$) with the driving frequency of 0.5 Hz of LaCe-based BMGs.

BMG Composition	Dc (mm) [32]	T_g (K) [32]	T_x (K) [32]	ΔT_x (K) [32]	T_{rg} [32]	Γ [32]	$Q_p{}^{-1}$	$Q_i{}^{-1}$
$(La_{0.3}Ce_{0.7})_{65}Al_{10}Co_{25}$	9	416	436	20	0.54	0.365	0.28	0.19
$(La_{0.5}Ce_{0.5})_{65}Al_{10}Co_{25}$	15	427	453	26	0.55	0.376	0.42	0.27
$(La_{0.6}Ce_{0.4})_{65}Al_{10}Co_{25}$	20	437	467	30	0.52	0.367	0.53	0.37
$(La_{0.7}Ce_{0.3})_{65}Al_{10}Co_{25}$	25	437	472	35	0.51	0.367	0.56	0.44
$(La_{0.8}Ce_{0.2})_{65}Al_{10}Co_{25}$	12	439	476	37	0.50	0.364	0.51	0.29

The GFA data listed in Table 1 and the data illustrated in Figure 3a,b imply that the peak of Q^{-1} ($Q_P{}^{-1}$) is correlated with the GFA of LaCe-based BMGs. The GFA and $Q_P{}^{-1}$ of $(La_{0.7}Ce_{0.3})_{65}Al_{10}Co_{25}$ BMG are the largest among LaCe-based BMGs, and a 25 mm-diameter rod with a fully amorphous structure can be obtained [32]. Our previous investigation revealed that the inflection point that appears before the IF peak indicates the onset temperature of crystallization, and the IF value of the inflection point on the Q^{-1}–T curve is defined as $Q_i{}^{-1}$ [35]. As shown in Table 1, the $Q_P{}^{-1}$ and $Q_i{}^{-1}$ values of $(La_{0.7}Ce_{0.3})_{65}Al_{10}Co_{25}$ BMG are the largest among the LaCe-based BMGs. The $Q_P{}^{-1}$ and $Q_i{}^{-1}$ values with a frequency of 0.5 Hz are 0.56 and 0.44, respectively. These experimental results initially reveal that the GFA of the LaCe-based BMGs can be determined by the $Q_P{}^{-1}$ and $Q_i{}^{-1}$ values. At the same driving frequency, the LaCe-based BMG with good GFA shows large $Q_P{}^{-1}$ and $Q_i{}^{-1}$ values.

Empirical GFA criteria, such as ΔT_x, T_{rg}, and γ, are determined on the basis of previously described procedures [32] to verify the reliability of the new GFA criterion (Table 1). Table 1 indicates that ΔT_x is in accordance with the GFA of LaCeAlCo BMGs; however, the ΔT_x of $(La_{0.8}Ce_{0.2})_{65}Al_{10}Co_{25}$ is inconsistent with the GFA. For other GFA criterions, such as T_{rg} and the parameter γ, the values are inconsistent with the variation tendency of GFA. Figure 3 shows that the variation tendency of $Q_P{}^{-1}$ is approximately coincident with that of GFA. The comparison of $Q_P{}^{-1}$ and GFA reveals their small deviation between $(La_{0.4}Ce_{0.6})_{65}Al_{10}Co_{25}$ BMG and $(La_{0.8}Ce_{0.2})_{65}Al_{10}Co_{25}$ BMG. The variation tendency of $Q_i{}^{-1}$ is slightly consistent with that of the GFA. Hence, the GFA of LaCe-based BMGs can be determined by using $Q_i{}^{-1}$.

The IF of a series of ZrCu- and La-based BMGs with different GFAs was measured to verify the validity of $Q_i{}^{-1}$ for other BMG alloy systems. The Q^{-1}–T curves are presented in Figure 4a,b, and the $Q_P{}^{-1}$ and $Q_i{}^{-1}$ values are listed in Table 2. As shown in Table 2, the ZrCu-based BMG with the highest GFA is $Zr_{46}Cu_{30.14}Ag_{8.36}Al_8Be_{7.5}$, and a 73-mm rod with a fully amorphous structure can be formed [29]. The $Q_i{}^{-1}$ of $Zr_{46}Cu_{30.14}Ag_{8.36}Al_8Be_{7.5}$ BMG in Figure 4a is 4.758, which is the highest among all studied BMGs. As shown in Figure 4b and Table 2, the La-based BMG with the highest GFA is $La_{65}Al_{14}Cu_{9.167}Ag_{1.833}Ni_5Co_5$, and a 30-mm rod with a fully amorphous structure can be formed [31]. The $Q_i{}^{-1}$ value derived from Figure 4b is 1.146, which is the highest $Q_i{}^{-1}$ value among all the studied La-based BMGs. This finding indicates a positive relationship between $Q_i{}^{-1}$ and GFA for LaCe-, ZrCu-, and La-based BMGs. In a certain alloy system, the GFA of BMGs can be determined by the $Q_i{}^{-1}$ value. Under the same heating rate and driving frequency, $Q_i{}^{-1}$ and GFA are directly proportional to each other.

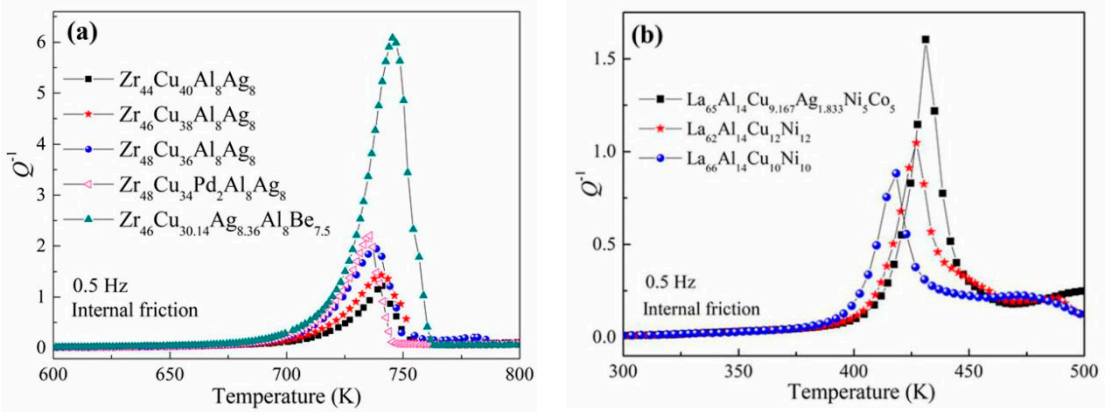

Figure 4. (**a**) Q^{-1}–T curves of a series of Zr-based BMGs with a driving frequency of 0.5 Hz; (**b**) Q^{-1}–T curves of a series of La-base BMGs with a driving frequency of 0.5 Hz.

Table 2. The GFA value (determined by the critical parameter [28–31]), IF peak values ($Q_p{}^{-1}$) with a driving frequency of 0.5 Hz, and inflection point IF values ($Q_i{}^{-1}$) with a driving frequency of 0.5 Hz of Zr-based BMGs and La-based BMGs.

BMG Composition	D_c (mm)	$Q^{-1}{}_p$	$Q^{-1}{}_i$
$Zr_{44}Cu_{40}Al_8Ag_8$	15 [28]	1.215	0.937
$Zr_{46}Cu_{38}Al_8Ag_8$	20 [28]	1.428	1.064
$Zr_{48}Cu_{36}Al_8Ag_8$	25 [28]	1.943	1.569
$Zr_{48}Cu_{34}Pd_2Al_8Ag_8$	30 [28]	2.202	1.697
$Zr_{46}Cu_{30.14}Ag_{8.36}Al_8Be_{7.5}$	73 [29]	6.081	4.758
$La_{66}Al_{14}Cu_{10}Ni_{10}$	8 [30]	0.883	0.495
$La_{62}Al_{14}Cu_{12}Ni_{12}$	12 [28]	1.046	0.677
$La_{65}Al_{14}Cu_{9.167}A_{g1.833}Ni_5Co_5$	30 [31]	1.604	1.146

4. Discussion

During the quenching of glass formation, numerous quenched materials occur in free volumes, and the atomic clusters distributed around the free volumes can be regarded as the structural units for the structure relaxation of BMGs [4]. These clusters are metastable, and the atomic mobility is active in these "units". With the thermal activation accompanied by an elevated temperature, the atomic movement inside the BMGs is increased and thus induces relaxation from a metastable to stable state [36]. When the temperature increases to the supercooled liquid region, the atomic number involved in the relaxation is also increased, and the thermal-activated movement is intensified. As a result, apparent strain occurs behind stress and manifests externally as the increase in Q^{-1} of the BMGs [3–5]. Furthermore, a large supercooled liquid region is a common feature of BMGs; such a wide temperature range allows the BMGs to be maintained in this state for a long time to ensure that the Q^{-1} increases steadily until crystallization occurs. The IF in the supercooled liquid region can be related to viscosity. Wang et al. [37] proposed the approximate formula:

$$Q_{liq}^{-1} = G_u/\omega\eta \tag{1}$$

where G_u is the un-relaxed modulus, and ω is the circular frequency. The equilibrium viscosity of the supercooled liquid for BMGs is usually expressed with the Vogel–Fulcher–Tammann (VFT) relation [37,38]:

$$\eta = \eta_0 \exp(D^* T_0/(T - T_0)) \tag{2}$$

where η_0 is the high temperature limit of the viscosity, D^* corresponds to the strength parameter, and T_0 is the VFT temperature. By introducing Equation (2) to Equation (1), the IF in the supercooled liquid region can be expressed as:

$$Q_{liq}^{-1} = G_u/\omega\eta_0 \exp(D^* T_0/(T - T_0)) \tag{3}$$

The η_0 and D^* values are different for the BMGs with different GFAs, especially for the BMGs with different constituting elements. The wide supercooled liquid region is a necessary condition for the high GFA and $Q_i{}^{-1}$ of BMGs; furthermore, the magnitude of D^* also has an important influence on the $Q_i{}^{-1}$ value. The BMG melts, which has a large D^*, and usually has a high stability of the disordered liquid, and the glassy solid easily forms during the cooling process. Hence, the magnitude of the $Q_i{}^{-1}$ value is determined by the width of the supercooled liquid region and the basic attribute of the alloy melt. A comparison of the GFA of BMGs shows that the magnitude of the $Q_i{}^{-1}$ value has a high reliability.

By differentiating Equation (3) with respect to the temperature, one can obtain the variation tendency of Q^{-1} in the supercooled liquid region, which can be expressed as follows [35]:

$$(Q_{liq}^{-1})' = G_u D^* T_0/\omega\eta_0 (T - T_0)^2 \exp(D^* T_0/(T - T_0)) \tag{4}$$

The differential curve of Q_{liq}^{-1} is an increasing function. The results indicate that in the supercooled liquid region, the IF will increase continuously with an elevating temperature.

Whenever crystallization occurs, the IF will be the sum of Q_{liq}^{-1} and Q_x^{-1}, where Q_x^{-1} represents the IF of the crystalline phase of the corresponding BMG. Q_x^{-1} usually has orders of magnitude of 10^{-2}–10^{-3} and changes slightly with an elevating temperature. The IF of the crystalized BMGs, which involves Q_{liq}^{-1} and Q_x^{-1}, can be expressed as follows [23,35]:

$$Q^{-1} = (1 - X(T))G_u/\omega\eta_0 \exp(D^*T_0/(T - T_0)) + X(T)Q_x^{-1} \quad (5)$$

where *X(T)* is the crystallized fraction. The results imply that the increasing of the crystallized fraction *X(T)* will break the rising tendency of the IF with an elevating temperature. Given the small order of magnitude of Q_x^{-1}, the onset of the crystallization will break the increasing tendency of the Q_{liq}^{-1}. As a result, an inflection point will appear on the Q^{-1}–T curve before the IF peak appears. Thus, the supercooled liquid region ends up with an inflection point in the Q^{-1}–T curve.

For example, the derivation of the Q^{-1}–T curve of $(La_{0.5}Ce_{0.5})_{65}Al_{10}Co_{25}$ BMG reveals the derivative plots (Figure 5) and indicates the increasing rate of the IF of BMGs. The increment in the speed of IF is fast at the inflection point, so the hysteresis rate between stress and strain is the fastest at this point; that is, the minimum duration required for mechanical relaxation is obtained at this point. In the subsequent heating, the derivative is positive, so Q^{-1} increases. However, the derivative decreases from the maximum value to zero in the narrow temperature range from the inflection point to the IF peak. In Equations (3) and (4), the IF of the BMGs in the supercooled liquid region increases gradually, but an IF peak never appears unless the internal state of BMGs changes. In other words, the appearance of IF peak is the result of crystallization, and the onset of crystallization most likely starts from the inflection point. Technically, a supercooled liquid region ends up at an inflection point. Q_i^{-1} accurately reflects the maximum Q^{-1} of BMGs in an amorphous state. However, Q_P^{-1} is affected by crystallization and cannot reflect the whole state of amorphous BMGs.

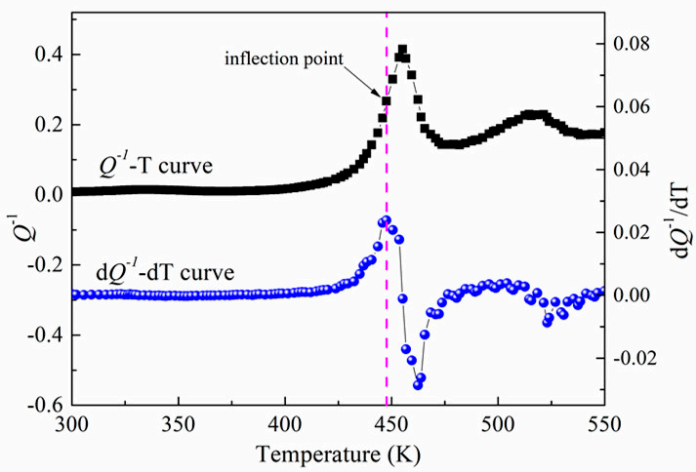

Figure 5. The Q^{-1}-T curve and dQ^{-1}/dT-T curve of $(La_{0.5}Ce_{0.5})_{65}Al_{10}Co_{25}$ BMG with a frequency of 0.5 Hz.

The physical model of Q^{-1} in a supercooled state, which is composed of amorphous and crystallized fractions and is expressed in Equation (5), shows that Q_P^{-1} can be regarded as the sum of Q^{-1} of the residual BMG and Q^{-1} of the crystallized fraction. Q_P^{-1} is composed of a portion of Q_x^{-1}, and the relationship between Q_P^{-1} and GFA of BMGs weakens because of crystallization. Hence, the GFA of BMGs with the same alloy system can be determined on the basis of Q_i^{-1}. GFA is exceptional when Q_i^{-1} is large.

The nature of IF is considered as the result of stress relaxation [39,40], which is embodied as the transition of the local structures, induced by an external stress, from metastable states to stable states. The peak value of Q^{-1} is related to the disordered amorphous structure and relaxation process in the

supercooled liquid state upon heating. Q_i^{-1} of the BMGs with different GFAs is significantly different, involving different ΔT_x values. By taking Q_i^{-1} as the vertical axis and ΔT_x as the horizontal axis, the relationship of all of the LaCe-, ZrCu-, and La-based BMGs can be determined, as listed in Figure 6. Figure 6 shows that the Q_i^{-1} value is directly proportional to the GFA of the BMGs; that is, the higher the GFA, the larger the Q_i^{-1} value. Comparing the GFA of BMGs by using Q_i^{-1} is valid among the same alloy systems. Thus, Q_i^{-1} can only be used to evaluate the GFA of the BMGs if the constituent elements are the same. Given the difference of constituent elements among different alloy systems, the differences in characteristic parameters are significant, such as the modulus, ΔT_x, and D^* value, which causes a significant difference in the Q_i^{-1} value determined by the IF measurement, as shown in Figure 6.

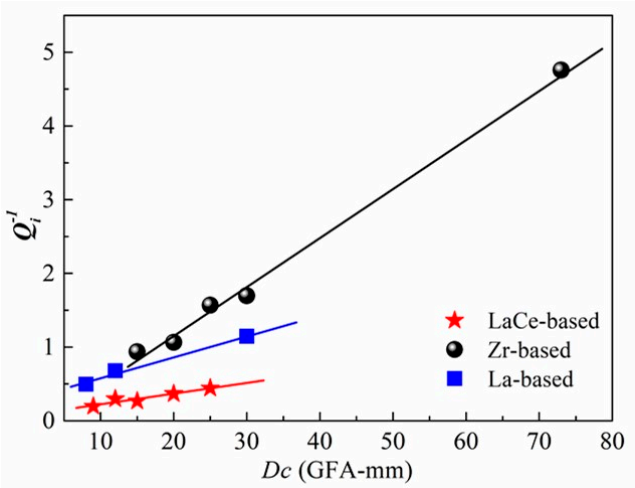

Figure 6. Relationship of GFA and the Q_i^{-1} magnitude for LaCe-based, Zr-based, and La-based BMGs.

5. Conclusions

On the basis of the results of IF measurements for different BMG systems, we proposed a new method for determining the GFA of BMGs within a single alloy system by using an IF measurement. Q_i^{-1} of the inflection point of the Q^{-1}–T curve that lies on the left of the IF peak can be used to determine the GFA of BMGs. The larger Q_i^{-1} is, the better the GFA will be. A comparison of the GFA by using the Q_i^{-1} value is valid for BMG systems with similar main constituent elements. The magnitude of Q_i^{-1} is believed to be related to ΔT_x, given that ΔT_x is an efficient criterion of GFA. The Q_i^{-1} value is believed to be a valid criterion under certain conditions; that is, constituent elements are identical, and element contents are different. Differences in Q_i^{-1} of BMGs in different alloy families may be significant, so Q_i^{-1} may be unreliable, and one may need further studies to explain its unreliability and to find a generalized criterion.

Author Contributions: X.Z. (Xianfeng Zhang) conceptualization, date curation, formal analysis, methodology, software, writing-original draft, writing—review and editing. X.C. conceptualization, investigation, project administration, resources, visualization, writing—original draft. Z.D. methodology, resources. F.Z. funding acquisition, project administration, resources. J.L. writing—review and editing. B.B. visualization. K.X. writing—review and editing. X.Z. (Xinyao Zhang) writing—review and editing. All authors have read and agreed to the published version of the manuscript.

Funding: This research was funded by the Major Agricultural Application Technology Innovation Projects in Shandong Province (Grant No. SD2019NJ017), and the National Natural Science Foundation of China (Grant No. 50971053).

Conflicts of Interest: The authors declare no conflict of interest.

References

1. Wang, L.T.; Ge, T.S. Nonlinear internal friction in Mn-Cu Martensite. *Phys. Status Solidi A* **1988**, *105*, 447–453. [CrossRef]
2. Khonik, V.A.; Spivak, L.V. On the nature of low temperature internal friction peaks in metallic glasses. *Acta Mater.* **1996**, *44*, 367–381. [CrossRef]
3. Sinning, H.R. Low-frequency internal friction of metallic glasses near Tg-A critigue of the use of the torsion pendulum. *J. Non-Cryst. Solids* **1989**, *110*, 195–202. [CrossRef]
4. He, Y.H.; Li, X.G. A new type of internal-friction peak of metallic glasses near Tg. *Phys. Status Solidi A* **1987**, *99*, 115–120.
5. Barmatz, M.; Chen, H.S. Youngs modulus and internal-friction in metallic glass alloys from 1.5 to 300K. *Phys. Rev. B* **1974**, *9*, 4073–4083. [CrossRef]
6. Hiki, Y.; Tanahashi, M.; Takeuchi, S. Stabilization of metallic glass studied by internal friction measurement. *J. Non-Cryst. Solids* **2008**, *354*, 1780–1785. [CrossRef]
7. Cui, X.; Zhang, X.F.; Meng, L.Z.; Guo, J.; Ma, Y.B.; Meng, X.J.; Bian, B.C.; Zhao, R.G.; Zu, F.Q. Analysis of β relaxation using internal friction measurement and mechanical testing for a LaCe-based bulk metallic glass. *J. Non-Cryst. Solids* **2019**, *525*, 119670. [CrossRef]
8. Jung, I.C.; Kang, D.G.; De Cooman, B.C. Impulse Excitation Internal Friction Study of Dislocation and Point Defect Interactions in Ultra-Low Carbon Bake-Hardenable Steel. *Metall. Mater. Trans. A* **2014**, *45*, 1962–1978. [CrossRef]
9. Fang, Q.F.; Ge, T.S. Low temperature internal friction peaks associated with the interaction between dislocations and point defects in dilute aluminium-magnesium solid solutions. *Acta Metall. Mater.* **1990**, *38*, 419–424. [CrossRef]
10. Sun, M.; Wang, X.P.; Wang, L.; Wang, H.; Jiang, W.B.; Liu, W.; Hao, T.; Gao, R.; Gao, Y.X.; Zhang, T.; et al. High-temperature order-disorder phase transition in Fe-18Ga alloy evaluated by internal friction method. *J. Alloys Compd.* **2018**, *750*, 669–676. [CrossRef]
11. Wu, Y.X.; Hao, T.; Sun, M.; Jiang, W.B.; Wang, X.P.; Fang, Q.F.; Liu, X.B.; Li, Y.F.; Xue, F. Internal friction study on precipitation/dissolution of Mn-Ni-Si phase in aged RPV model steel. *Matter. Lett.* **2020**, *269*, 127668. [CrossRef]
12. Khonik, V.; Kobelev, N. Metallic Glasses: A New Approach to the Understanding of the Defect Structure and Physical Properties. *Metals* **2019**, *9*, 605. [CrossRef]
13. Nemilov, S.V. The review of possible interrelations between ionic conductivity, internal friction and the viscosity of glasses and glass forming melts within the framework of Maxwell equations. *J. Non-Cryst. Solids* **2011**, *357*, 1243–1263. [CrossRef]
14. Qiao, J.C.; Ren, T.P.; Lyu, G.J.; Zhang, L.; Zhang, H.F.; Pelletier, J.M.; Yao, Y. Physical mechanism of internal friction behavior of beta-type bulk metallic glass composites. *Mater. Sci. Eng. A* **2019**, *739*, 193–197. [CrossRef]
15. Hockicko, P.; Mizerakova, J.; Munoz, F. The internal friction of lithium and sodium borophosphate glasses. *J. Non-Cryst. Solids* **2018**, *498*, 194–198. [CrossRef]
16. Fursova, Y.V.; Khonik, V.A. Viscoelastic infralow-frequency internal friction as a result of irreversible structural relaxation of a metallic glass. *Philos. Mag. A* **2000**, *80*, 1855–1865. [CrossRef]
17. Tan, M.; He, Y.Z. Internal friction behaviour of metallic glass Cu70Ti30 during structural relaxation and crystallization. *J. Non-Cryst. Solids* **1988**, *105*, 155–161.
18. Liu, C.R.; Pineda, E.; Crespo, D.; Qiao, J.C.; Evenson, Z.; Ruta, B. Sub-Tg relaxation times of the alpha process in metallic glasses. *J. Non-Cryst. Solids* **2017**, *471*, 322–327. [CrossRef]
19. Ding, H.L.; Xie, Z.M.; Fang, Q.F.; Zhang, T.; Cheng, Z.J.; Zhuang, Z.; Wang, X.P.; Liu, C.S. Determination of the DBTT of nanoscale ZrC doped W alloys through amplitude-dependent internalfriction technique. *Mater. Sci. Eng. A* **2018**, *716*, 268–273. [CrossRef]
20. Morito, N.; Egami, T. Internal-friction and reversible structure relaxation in the metallic-glass $Fe_{32}Ni_{36}Cr_{14}P_{12}B_6$. *Acta Metall.* **1984**, *32*, 603–613. [CrossRef]
21. Morito, N.; Egami, T. Correlation of the shear modulus and internal-friction in the reversible structural relaxation of a glassy metal. *J. Non-Cryst. Solids* **1984**, *61–62*, 973–978. [CrossRef]

22. Yang, K.W.; Jia, E.G.; Shui, J.P.; Zhu, Z.G. Crystallization study of amorphous Pd43Ni10CU27P20 alloy by internal friction measurement. *Phys. Status Solidi A* **2007**, *204*, 3297–3304. [CrossRef]
23. Zhang, B.; Zu, F.Q.; Zhen, K.; Shui, J.P.; Wen, P. Internal friction behaviours in Zr57Al10Ni12.4Cu15.6Nb5 bulk metallic glass. *J. Phys. D Condens. Matter.* **2002**, *14*, 7461–7470. [CrossRef]
24. Inoue, A.; Zhang, T.; Masumoto, T. Glass-forming ability of alloys. *J. Non-Cryst. Solids* **1993**, *156*, 473–480. [CrossRef]
25. Turnbull, D. Under what conditions can a glass be formed. *Contemp. Phys.* **1969**, *10*, 473. [CrossRef]
26. Lu, Z.P.; Liu, C.T. A new glass-forming ability criterion for bulk metallic glasses. *Acta Mater.* **2002**, *50*, 3501–3512. [CrossRef]
27. Wang, L.F.; Zhang, Q.D.; Cui, X.; Zu, F.Q. An empirical criterion for predicting the glass-forming ability of amorphous alloys based on electrical transport properties. *J. Non-Cryst. Solids* **2015**, *419*, 51–57. [CrossRef]
28. Long, Z.L.; Wei, H.Q.; Ding, Y.H.; Zhang, P.; Xie, G.Q.; Inoue, A. A new criterion for predicting the glass-forming ability of bulk metallic glasses. *J. Alloys Compd.* **2009**, *475*, 207–219. [CrossRef]
29. Lou, H.B.; Wang, X.D.; Xu, F.; Ding, S.Q.; Cao, Q.P.; Hono, K.; Jiang, J.Z. 73 mm-diameter bulk metallic glass rod by copper mould casting. *Appl. Phys. Lett.* **2011**, *99*, 051910. [CrossRef]
30. Luo, Q.; Wang, W.H. Rare earth based bulk metallic glasses. *J. Non-Cryst. Solids* **2009**, *355*, 759–775. [CrossRef]
31. Jiang, Q.K.; Zhang, G.Q.; Yang, L.; Wang, X.D.; Saksl, K.; Franz, H.; Wunderlich, R.; Fecht, H.; Jiang, J.Z. La-based bulk metallic glasses with critical diameter up to 30 mm. *Acta Mater.* **2007**, *55*, 4409–4418. [CrossRef]
32. Li, R.; Pang, S.J.; Ma, C.L.; Zhang, T. Influence of similar atom substitution on glass formation in (La–Ce)–Al–Co bulk metallic glasses. *Acta Mater.* **2007**, *55*, 3719–3726. [CrossRef]
33. Liu, M.N.; Qiao, J.C.; Hao, Q.; Chen, Y.H.; Yao, Y.; Crespo, D.; Pelletier, J.M. Dynamic Mechanical Relaxation in LaCe-Based Metallic Glasses: Influence of the Chemical Composition. *Metals* **2019**, *9*, 1013. [CrossRef]
34. Qiao, J.C.; Wang, Q.; Pelletier, J.M.; Kato, H.; Casalini, R.; Crespo, D.; Pineda, E.; Yao, Y.; Yang, Y. Structural heterogeneities and mechanical behavior of amorphous alloys. *Prog. Mater. Sci.* **2019**, *104*, 250–329. [CrossRef]
35. Cui, X.; Zu, F.Q.; Wang, L.F.; Wang, Z.Z.; Li, X.Y.; Huang, Z.Y. A method for determining the crystallization temperature in studying internal friction behaviors of bulk metallic glasses. *J. Non-Cryst. Solids* **2013**, *366*, 59–63. [CrossRef]
36. Yu, H.B.; Wang, W.H.; Bai, H.Y.; Samwer, K. The β-relaxation in metallic glasses. *Natl. Sci. Rev.* **2014**, *1*, 429–461. [CrossRef]
37. Wang, Q.; Lu, J.; Gu, F.J.; Xu, H.; Dong, Y.D. Isothermal internal friction behaviour of a Zr based bulk metallic glass with large supercooled liquid region. *J. Phys. D Appl. Phys.* **2006**, *39*, 2851–2855. [CrossRef]
38. Busch, R.; Masuhr, A.; Johnson, W.L. Thermodynamics and kinetics of Zr-Ti-Cu-Ni-Be bulk metallic glass forming liquids. *Mater. Sci. Eng. A* **2001**, *304–306*, 97–102. [CrossRef]
39. Qiao, J.C.; Wang, Y.J.; Pelletier, J.M.; Keer, L.M.; Fine, M.E.; Yao, Y. Characteristics of stress relaxation kinetics of La60Ni15Al25 bulk metallic glass. *Acta Mater.* **2015**, *98*, 43–50. [CrossRef]
40. Qiao, J.C.; Wang, Y.J.; Zhao, L.Z.; Dai, L.H.; Crespo, D.; Pelletier, J.M.; Keer, L.M.; Yao, Y. Transition from stress-driven to thermally activated stress relaxation in metallic glasses. *Phys. Rev. B* **2016**, *94*, 104203. [CrossRef]